

Universal scaled Higgs-mass gap for the bilayer Heisenberg model in the ordered phase

Yoshihiro Nishiyama

Department of Physics, Faculty of Science, Okayama University, Okayama 700-8530, Japan

Received: date / Revised version: date

Abstract. The spectral properties for the bilayer quantum Heisenberg model were investigated with the numerical diagonalization method. In the ordered phase, there appears the massive Higgs excitation embedded in the continuum of the Goldstone excitations. Recently, it was claimed that the *properly scaled* Higgs mass is a universal constant in proximity to the critical point. Diagonalizing the finite-size cluster with $N \leq 36$ spins, we calculated the dynamical scalar susceptibility $\chi_s''(\omega)$, which is rather insensitive to the Goldstone mode. A finite-size-scaling analysis of $\chi_s''(\omega)$ is made, and the universal (properly scaled) Higgs mass is estimated.

PACS. 75.10.Jm Quantized spin models – 05.70.Jk Critical point phenomena – 75.40.Mg Numerical simulation studies – 05.50.+q Lattice theory and statistics (Ising, Potts, etc.)

1 Introduction

In the spontaneous-symmetry-breaking phase, there appear the Goldstone and Higgs excitations in the low-energy spectrum. The former (latter) excitation is massless (massive), and the continuum of the former overwhelms the latter dispersion branch. [In regard to the wine-bottle bottom potential, the former (latter) excitation corresponds to the azimuthal (radial) modulation of the order param-

eter concerned.] Recently, the Higgs-excitation spectral peak was observed for the the two-dimensional ultra-cold atom [1]. Here, a key ingredient is that the external disturbance, namely, the trap-potential modulation, retains the U(1) (gauge) symmetry, and it is rather insensitive to the (low-lying) Goldstone modes. Moreover, the experiment revealed a gradual closure of the Higgs mass m_H in proximity to the critical point between the superfluid and Mott-insulator phases; the criticality belongs to the $(2+1)$ -dimensional O(2) universality class, and the singu-

Send offprint requests to:

larity lies out of the scope of the Ginzburg-Landau theory. Such O(2)- [equivalently, U(1)-] symmetric system is ubiquitous in nature, and the underlying physics is common to a wide variety of substances; we refer readers to Ref. [2] for a review.

In this paper, we investigate the O(3)-symmetric counterpart, namely, the bilayer quantum Heisenberg model [3, 4, 5], by means of the numerical diagonalization method. Our aim is to estimate the scaled Higgs mass (universal amplitude ratio) m_H/Δ (Δ : the excitation gap in the adjacent paramagnetic phase); technical details are addressed in Sec. 2. The scaled Higgs mass has been estimated as $m_H/\Delta = 2.2(3)$ [6] and $2.6(4)$ [7] with the (quantum) Monte Carlo method. On the one hand, via the elaborated renormalization-group analyses, the scaled Higgs mass was estimated as $m_H/\Delta = 2.7$ [8] and 1.64 [9]. An advantage of the numerical diagonalization approach is that the spectral property is accessible directly [10] without resorting to the inverse Laplace transformation (see Appendix B of Ref. [11]). It has to be mentioned that the scaled Higgs mass m_H/Δ has been investigated extensively as for the O(2)-symmetric case, [6, 8, 9, 11, 12, 13, 14]. According to the study [13] of the O(N)-symmetric system with generic N , the Higgs-excitation peak should get broadened for large N .

To be specific, we present the Hamiltonian for the bilayer Heisenberg model [3, 4, 5]

$$\mathcal{H} = -J \sum_{a=1}^2 \sum_{\langle ij \rangle} \mathbf{S}_{ai} \cdot \mathbf{S}_{aj} + J' \sum_{i=1}^{N/2} \mathbf{S}_{1i} \cdot \mathbf{S}_{2i}. \quad (1)$$

Here, the spin- $S = 1/2$ operator \mathbf{S}_{ai} is placed at each square-lattice point i ($i = 1, 2, \dots, N/2$) within each layer a ($a = 1, 2$). The summation $\sum_{\langle ij \rangle}$ runs over all possible nearest neighbor pairs $\langle ij \rangle$ within each layer. The parameter $J(> 0)$ [$J'(> 0)$] denotes the intra- (inter-) layer ferromagnetic (antiferromagnetic) Heisenberg interaction; hereafter, we consider J' as the unit of energy ($J' = 1$). The phase diagram [3] is presented in Fig. 1. At $J_c = 0.435$ [4], there occurs a phase transition, separating the paramagnetic ($J < J_c$) and ordered ($J > J_c$) phases; the phase transition belongs to the three-dimensional O(3) universality class [4]. The criticality of the spectral function in the ordered phase is our concern. It has to be mentioned that the recent quantum Monte Carlo simulation [7] also treats the bilayer Heisenberg model (1), albeit with an antiferromagnetic intra-layer interaction, $J < 0$. The setting of the interaction parameter may be arranged suitably for each methodology. Nevertheless, details of magnetism should not influence the criticality of m_H .

The rest of this paper is organized as follows. In Sec. 2, we analyze the spectral properties for the Hamiltonian (1) by means of the numerical diagonalization method. The simulation algorithm is presented in Appendix. In Sec. 3, we address the summary and discussions.

2 Numerical results

In this section, we present the numerical results. We employed the numerical diagonalization method for the finite-size cluster with $N \leq 36$ spins. We implemented the screw-boundary condition (Appendix) [15] in order to treat a

variety of $N = 30, 32, \dots$ systematically. Because the N spins constitute the bilayer cluster, the linear dimension of the cluster is given by

$$L = \sqrt{N/2}. \quad (2)$$

2.1 Finite-size-scaling analysis of the Goldstone mass

m_G

As a preliminary survey, we analyze the Goldstone mass m_G with the finite-size-scaling method. The Goldstone mass m_G is identified as the triplet (magnon) excitation gap; hence, the simulation was performed within the subspace specified by the longitudinal total magnetization, either $S_{tot}^z = 0$ or 1.

In Fig. 2, we present the scaled Goldstone mass Lm_G for various J and system sizes, $N(= 2L^2) = 30$ (+), 32 (\times) 34 (*) and 36 (\square). The data suggest that a phase transition takes place at $J \approx 0.4$; note that the intersection point of the curves indicates the location of the critical point. In Ref. [4], the critical point was estimated as $J_c = 0.435$; our result agrees with this estimate. The Goldstone mass appears to close, $m_G[< O(L^{-1})] \rightarrow 0$, in the ordered phase $J > J_c$ as $L \rightarrow \infty$ (thermodynamic limit). On the contrary, in the paramagnetic phase $J < J_c$, a finite mass gap opens; in the quantum-magnetism language, the mass gap is interpreted as the spin (magnon) gap for the spin-liquid phase. The spin gap [see Eq. (5)] sets a fundamental energy scale for the subsequent scaling analyses.

In Fig. 3, we present the scaling plot for the Goldstone mass, $(J - J_c)L^{1/\nu} - Lm_G$, for various J and system sizes,

$N = 30$ (+), 32 (\times) 34 (*) and 36 (\square). Here, the scaling parameters, $J_c = 0.435$ and $\nu = 0.7112$, are taken from Refs. [4] and [16, 17], respectively; namely, there are no adjustable parameters involved in the scaling analysis. From Fig. 3, we see that the data collapse into a scaling curve satisfactorily for a considerably wide range of J . Such a feature indicates that the simulation data already enter the scaling regime. Encouraged by this finding, we turn to the analysis of the spectral properties.

2.2 Spectral function (dynamical scalar susceptibility)

$\chi_s''(\omega)$

In Fig. 4, we present the spectral function (dynamical scalar susceptibility) [18]

$$\chi_s''(\omega) = -\frac{1}{N} \text{Im} \left\langle g \left| \mathcal{E}^\dagger \frac{1}{\mathcal{H} - E_g - \omega + i\delta} \mathcal{E} \right| g \right\rangle, \quad (3)$$

for various ω with fixed $J = 0.8 (> J_c)$ and $N = 36$. The energy-resolution parameter is set to $\delta = 1.4$ (solid) and 0.3 (dotted). Here, the symbol $|g\rangle$ (E_g) denotes the ground-state vector (energy), and the operator \mathcal{E} is given by $\mathcal{E} = \mathcal{P}\mathcal{H}|_{J=J_c}$ with the projection operator $\mathcal{P} = 1 - |g\rangle\langle g|$. The spectral function χ_s'' is sensitive (less sensitive) to the Higgs (Goldstone) mode, because the external perturbation \mathcal{E} retains the O(3) symmetry. An advantage of the numerical diagonalization approach is that the resolvent $f(z) = \langle g | \mathcal{E}^\dagger (\mathcal{H} - z)^{-1} \mathcal{E} | g \rangle$ is accessible directly via the continued-fraction expansion [10]. Actually, the continued-fraction-expansion method is essentially the same as that of the Lanczos diagonalization algorithm (tridiagonalization sequence), and computationally less de-

manding. The external perturbation \mathcal{E} is seemingly different from the conventional ones (implemented in the Monte Carlo simulations, for instance). However, as far as the symmetry is concerned, those choices are all equivalent, yielding an identical critical behavior as to m_H . Here, we employed the Hamiltonian itself as for \mathcal{E} , which turned out to be less influenced by corrections to scaling.

In Fig. 4 (solid), we observe a Higgs-excitation peak with the mass (excitation gap), $m_H = 2.2$. As mentioned above, the signal from the Higgs excitation comes up, because the scalar susceptibility χ_s'' is a good probe specific to it [18]; actually, there should exist low-lying ($0 < \omega < 2.2$) Goldstone and its continuum modes, as illustrated in Sec. 2.1. Above the threshold $\omega > 2.2$, a tail background extends. As mentioned afterward, the present simulation was performed so as to examine the main (Higgs) peak, and such high-lying spectral intensities are beyond the scope of the present analysis.

As a reference, we also presented a high-resolution result [Fig. 4 (dotted)], which reveals fine details of the spectral function, namely, the series of the constituent δ -function subpeaks. The Higgs peak splits into the primary and secondary subpeaks, which locate at $\omega = 1.9$ and 3.5 , respectively. As demonstrated in the next section, these fine structures (finite-size artifacts) have to be smeared out by an adequate δ in order to attain plausible finite-size-scaling behaviors.

Last, we address a number of remarks. First, as mentioned above, the Higgs peak consists of two subpeaks, and hence, it has an appreciable peak width. Such fea-

ture agrees with the claim [13] that the Higgs peak gets broadened for the $O(N)$ -symmetric model with large N . Last, rather technically, the continued-fraction expansion [10] was iterated until the above-mentioned secondary subpeak converges. The computational effort is comparable to that of the evaluation of $|g\rangle$.

2.3 Finite-size-scaling analysis of χ_s''

In this section, we analyze the finite-size-scaling behavior for χ_s'' in the ordered phase, $J > J_c$.

The spectral function obeys the finite-size-scaling formula [19]

$$\chi_s''(\omega) = L^{2/\nu-3} f[\omega/\Delta, (J - J_c)L^{1/\nu}], \quad (4)$$

with the critical point J_c , the correlation-length critical exponent ν , a certain scaling function f and the excitation gap

$$\Delta(J) = m_G(2J_c - J), \quad (5)$$

reflected as to the critical point J_c ; note that the Goldstone mass m_G was considered in Sec. 2.1. In other words, the Goldstone mode (in $J > J_c$) and the fundamental energy scale Δ (in $J < J_c$) continue adiabatically.

In Fig. 5, we present the scaling plot, $\omega/\Delta - L^{3-2/\nu} \chi_s''(\omega)$, for $N = 32$ (dotted), 34 (solid) and 36 (dashed) with fixed $\delta = 1.7\Delta$ and $(J - J_c)L^{1/\nu} = 2.5$. Here, the scaling parameters, $J_c = 0.435$ [4] and $\nu = 0.7112$ [17], are the same as those of Fig. 3; that is, there are no adjustable parameters in the scaling analysis. The scaled-spectral-function curves collapse into a scaling function f satisfactorily. From Fig. 5, we notice that the (properly scaled) Higgs mass takes

a universal value $m_H/\Delta = 2.7$. The universality (stability) of m_H/Δ with respect to the variation of the scaling argument $(J - J_c)L^{1/\nu}$ is examined in the next section.

2.4 Universal character of the scaled Higgs peak

In the above section, we investigated the universal behavior of χ_s'' (4) at a particular scaling argument, $(J - J_c)L^{1/\nu} = 2.5$, and observed a scaled Higgs mass $m_H/\Delta = 2.7$. In this section, we vary $(J - J_c)L^{1/\nu}$ in order to survey the universal character of the Higgs peak, particularly, the scaled Higgs mass.

In Fig. 6, we present the scaling plot, $\omega/\Delta - L^{3-2/\nu}\chi_s''(\omega)$, for various $(J - J_c)L^{1/\nu} = 2$ (dotted), 2.5 (solid) and 3 (dashed) with fixed $\delta = 1.7\Delta$ and $N = 36$; here, the scaling parameters, J_c and ν , are the same as those of Fig. 3. The data in Fig. 6 illustrate that the Higgs-peak position, $m_H/\Delta = 2.7$, is kept invariant with respect to the variation of $(J - J_c)L^{1/\nu}$. On the contrary, the Higgs-peak height seems to be scattered; note that according to Eq. (4), the Higgs peaks do not necessarily overlap, because a scaling argument $(J - J_c)L^{1/\nu}$ is no longer a constant value. In our preliminary survey, scanning the parameter space $(J - J_c)L^{1/\nu}$, we observed the following tendency. For $(J - J_c)L^{1/\nu} > 2$, the scaled Higgs mass $m_H/\Delta = 2.7$ is kept invariant. In closer look, however, for $(J - J_c)L^{1/\nu} > 3.5$, the Higgs peak drifts to the high-energy side gradually possibly because of the finite-size artifact (limitation of the tractable system size). The microscopic origin of the drift is as follows. The spectral weight transfers from the primary subpeak [see Fig. 4

(dotted)] to the secondary (and even ternary...) one(s) for $(J - J_c)L^{1/\nu} > 3.5$, and the Higgs peak drifts (and gets broadened); for exceedingly large $(J - J_c)L^{1/\nu}$, eventually, the simulation data may get out of the scaling regime. On the one hand, in the $(J - J_c)L^{1/\nu} < 2$ side, the Higgs mass acquires a significant enhancement. This narrow regime is not physically relevant, because the regime shrinks in the raw-parameter scale [like $J - J_c(< 2/L^{1/\nu}) \rightarrow 0$] as $L \rightarrow \infty$. To summarize, at least for the available system sizes $N \leq 36$, the scaling regime $(J - J_c)L^{1/\nu} \approx 2.5$ is optimal in the sense that the scaled Higgs mass takes a stable minimal value

$$m_H/\Delta = 2.7. \quad (6)$$

As mentioned above, the Higgs peak consists of two subpeaks. As a byproduct, we are able to estimate the intrinsic peak width. For $(J - J_c)L^{1/\nu} = 4.5$ and $N = 36$, these subpeaks locate at $\omega/\Delta \approx 2$ and 3.5 with almost identical spectral weights; hence, the center locates at $\omega/\Delta \approx 2.75$. The distance, 1.5, between these subpeaks may be a good indicator as to the intrinsic width of the Higgs peak, $\delta m_H/\Delta = 1.5$. It has been claimed [11] that the Higgs peak for the O(3)-symmetric model should be broadened significantly. Our result supports this claim.

3 Summary and Discussions

The criticality of the Higgs-excitation spectrum $\chi_s''(\omega)$ [Eq. (3)] for the bilayer Heisenberg model (1) was investigated by means of the numerical diagonalization method; the spectral function $\chi_s''(\omega)$ is accessible directly via the continued-

fraction expansion [10]. The spectral function appears to obey the scaling formula (4) satisfactorily, indicating that the simulation data already enter the scaling regime. As a result, we estimated the scaled Higgs mass $m_H/\Delta = 2.7$ with the peak width $\delta m_H/\Delta = 1.5$. So far, with the (quantum) Monte Carlo method, the scaled Higgs mass has been estimated as $m_H/\Delta = 2.2(3)$ [6] and $2.6(4)$ [7]. According to the normalization-group analysis, the scaled Higgs mass was estimated as $m_H/\Delta = 2.7$ [8] and 1.64 [9]. Our result agrees with these preceding estimates [6,7,8]; the error margin of our estimate should be bounded by half a peak width, ≈ 0.75 .

The Ginzburg-Landau theory (based on the wine-bottle-bottom potential) yields the critical amplitude ratio $m_H/\Delta = \sqrt{2}$. Clearly, the Ginzburg-landau theory fails in describing the spectral property for the $d = 3$ $O(3)$ universality class. In other words, such a spectral property reflects a character of each universality class rather sensitively. As a matter of fact, as for the “deconfined critical” phenomenon [20], an exotic spectral property was predicted. A consideration toward this direction is left for the future study.

Acknowledgment

This work was supported by a Grant-in-Aid for Scientific Research (C) from Japan Society for the Promotion of Science (Grant No. 25400402).

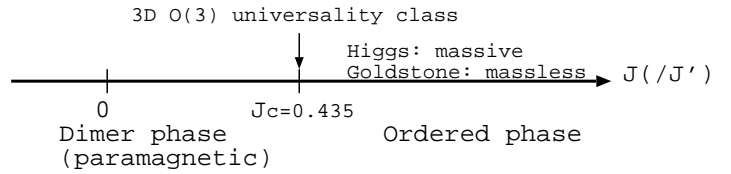


Fig. 1. A schematic phase diagram [3,4] for the bilayer Heisenberg model (1) is presented. A critical point locates at $J_c = 0.435$ [4], separating the paramagnetic and ordered phases. In the latter phase, the Higgs (Goldstone) excitation is massive (massless). The Higgs-excitation peak for the spectral function (3) is our concern.

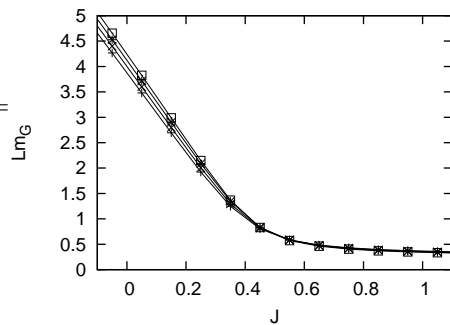


Fig. 2. The scaled Goldstone mass Lm_G is plotted for various J and $(+)$ $N(=2L^2) = 30$, (\times) 32, $(*)$ 34 and (\square) 36. The result agrees with the preceding estimate $J_c = 0.435$ [4]; note that the intersection point of the curves indicates the location of the critical point. In the ordered phase $J > J_c$, the Goldstone-excitation gap closes, $m_G[< O(L^{-1})] \rightarrow 0$, in the thermodynamic limit, $L \rightarrow \infty$. On the contrary, in the paramagnetic phase $J < J_c$, an excitation gap opens; the gap [see Eq. (5)] sets a fundamental energy scale for the subsequent scaling analyses.

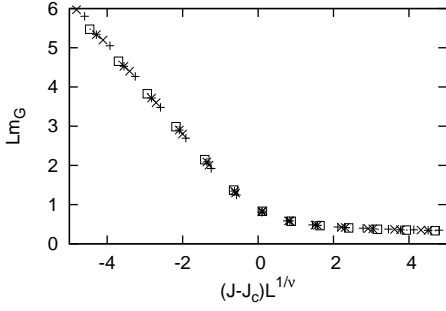


Fig. 3. The scaling plot for the Goldstone mass, $(J - J_c)L^{1/\nu} - Lm_G$, is plotted for (+) $N = 30$, (\times) 32 , ($*$) 34 and (\square) 36 . Here, the scaling parameters, $J_c = 0.435$ and $\nu = 0.7112$, are taken from the existing literatures, Refs. [4] and [16, 17], respectively. Namely, there are no adjustable parameters involved in the scaling analysis.

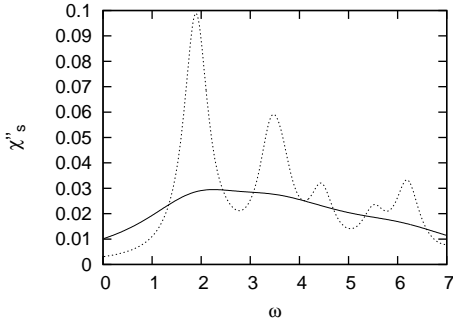


Fig. 4. The spectral function $\chi_s''(\omega)$ (3) is plotted for various ω with fixed $J = 0.8$ and $N = 36$. The ω -resolution parameter δ is set to $\delta = 1.4$ (solid) and 0.3 (dotted). The main peak at $\omega = 2.2$ (solid) corresponds to the Higgs excitation. The main peak consists of primary ($\omega = 1.9$) and secondary ($\omega = 3.5$) subpeaks; the Higgs-excitation peak acquires an intrinsic width.

A Numerical algorithm: Screw-boundary condition [15]

In this Appendix, we explain the simulation algorithm to diagonalize the Hamiltonian matrix for the bilayer Heisen-

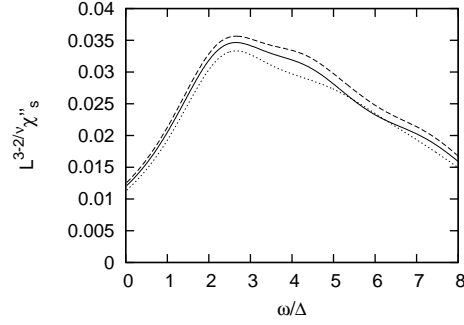


Fig. 5. The scaling plot (4) for the spectral function, $\omega/\Delta - L^{3-2/\nu} \chi_s''(\omega)$, is shown with fixed $(J - J_c)L^{1/\nu} = 2.5$ and $\delta = 1.7\Delta$ for various $N = 32$ (dotted), 34 (solid) and 36 (dashed); here, the scaling parameters, J_c and ν , are the same as those of Fig. 3. The scaled Higgs peak locates at $m_H/\Delta = 2.7$.

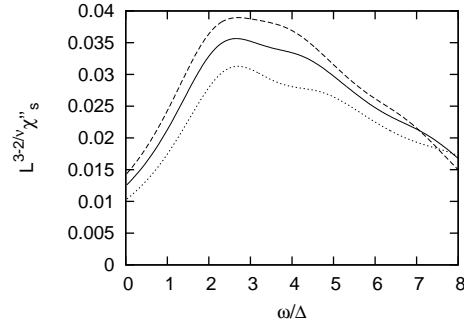


Fig. 6. The scaling plot (4) for the spectral function, $\omega/\Delta - L^{3-2/\nu} \chi_s''(\omega)$, is shown with fixed $N = 36$ and $\delta = 1.7\Delta$ for various scaling arguments $(J - J_c)L^{1/\nu} = 2$ (dotted), 2.5 (solid) and 3 (dashed); here, the scaling parameters, J_c and ν , are the same as those of Fig. 3. The curves do not necessarily overlap, because the scaling argument $(J - J_c)L^{1/\nu}$ is ranging. The scaled Higgs-peak position $m_H/\Delta = 2.7$ seems to be a universal constant.

berg model (1). We implemented the screw-boundary condition [15], with which one is able to treat a variety of system sizes $N = 30, 32, \dots$ (N : the number of constituent spins) systematically. According to Ref. [15], an alignment of spins σ_i ($i = 1, 2, \dots, M$) with both nearest-

and \sqrt{M} th-neighbor interactions is equivalent to a two-dimensional cluster under the screw-boundary condition; here, the periodical boundary condition as to the spin alignment, namely, $\sigma_{M+i} = \sigma_i$, is imposed. Based on this idea, we express the Hamiltonian matrix

$$\mathcal{H} = -J \sum_{a=1}^2 \sum_{i=1}^{N/2} (P^{-\sqrt{N/2}} \mathbf{S}_{ai} P^{\sqrt{N/2}}) \cdot \mathbf{S}_{ai} - J \sum_{a=1}^2 \sum_{i=1}^{N/2} \mathbf{S}_{a,i+1} \cdot \mathbf{S}_{ai} + J' \sum_{i=1}^{N/2} \mathbf{S}_{1i} \cdot \mathbf{S}_{2i},$$

with the translation operator (by one lattice spacing) P [15]; namely, a relation $P^{-\delta} \mathbf{S}_{ai} P^{\delta} = \mathbf{S}_{a,i+\delta}$ holds. We diagonalized the above Hamiltonian matrix (7) with the Lanczos method so as to evaluate the ground-state vector (energy) $|g\rangle$ (E_g). The above expression (7) is mathematically closed. However, as for an efficient simulation, a formula (11) of Ref. [21] may be of use in order to cope with the operation $P^{\pm\sqrt{N/2}}$.

References

1. M. Endres, T. Fukuhara, D. Pekker, M. Cheneau, P. Schauß, C. Gross, E. Demler, S. Kuhrand and I. Bloch, *Nature* **487** (2012) 454.
2. D. Pekker and C.M. Varma, *Annual Rev. Condens. Matter Phys.* **6** (2015) 269.
3. Y. Matsushita, M. P. Gelfand and C. Ishii, *J. Phys. Soc. Japan* **66** (1997) 3648.
4. M. Troyer and S. Sachdev, *Phys. Rev. Lett.* **81** (1998) 5418.
5. T. Sommer, M. Vojta and K. W. Becker, *Eur. Phys. J. B* **23** (2001) 329.
6. S. Gazit, D. Podolsky and A. Auerbach, *Phys. Rev. Lett.* **110** (2013) 140401.
7. M. Lohöfer, T. Coletta, D. G. Joshi, F. F. Assaad, M. Vojta, S. Wessel and F. Mila, arXiv:1508.07816.
8. F. Rose, F. Léonard and N. Dupuis, *Phys. Rev. B* **91** (2015) 224501.
9. Y. T. Katan and D. Podolsky, *Phys. Rev. B* **91** (2015) 075132.
10. E. R. Gagliano and C. A. Balseiro: *Phys. Rev. Lett.* **59** (1987) 2999.
11. S. Gazit, D. Podolsky, A. Auerbach and D. P. Arovas, *Phys. Rev. B* **88** (2013) 235108.
12. K. Chen, L. Liu, Y. Deng, L. Pollet and N. Prokof'ev, *Phys. Rev. Lett.* **110** (2013) 170403.
13. A. Rançon and N. Dupuis, *Phys. Rev. B* **89** (2014) 180501.
14. Y. Nishiyama, *Nucl. Phys. B* **897** (2015) 555.
15. M.A. Novotny, *J. Appl. Phys.* **67** (1990) 5448.
16. M. Hasenbusch, *J. Phys. A: Mathematical and General* **34** (2001) 8221.
17. M. Campostrini, M. Hasenbusch, A. Pelissetto, P. Rossi and E. Vicari, *Phys. Rev. B* **65** (2002) 144520.
18. D. Podolsky, A. Auerbach, and D. P. Arovas, *Phys. Rev. B* **84** (2011) 174522.
19. D. Podolsky and S. Sachdev, *Phys. Rev. B* **86** (2012) 054508.
20. Y. Huh, P. Strack and S. Sachdev, *Phys. Rev. Lett.* **111** (2013) 166401.
21. Y. Nishiyama, *Phys. Rev. E* **78** (2008) 021135.